Construction of compostable packaging with antibacterial property and improved performance using sprayed coatings of modified cellulose nanocrystals

Shuting Huang[1], Sheng Zou[1], Yixiang Wang[1,*]

[1] Department of Food Science and Agricultural Chemistry, McGill University, Ste Anne de Bellevue, Quebec, Canada H9X 3V9

* Correspondence: yixiang.wang@mcgill.ca, +001(514)3987922

Abstract

Increasing concerns about food safety and the environment have facilitated the development of eco-friendly antibacterial packaging. This study aimed to demonstrate a facile way to fabricate active packaging materials with modified cellulose nanocrystals (CNCs) and compare the effects of different modified CNCs on the performance of compostable materials. Polylactic acid (PLA) film was selected as a model, and CNCs were modified with methacrylamide, cetyltrimethylammonium bromide, and zinc oxide, respectively, and then applied on the surface of PLA films by spray-coating. All modified CNCs showed excellent antibacterial activity against *S. aureus* and *E. coli* (>99.999%). The effects of different CNC modifications on the performance of PLA films were investigated. Compared to neat PLA films, PLA/CNC films exhibited improved mechanical strength with maintained flexibility, lower gas permeability, and faster compost disintegration rate, and extended the shelf life of wrapped pork samples from 3 days to more than 10 days. Therefore, this work will also facilitate the applications of PLA materials in eco-friendly packaging.

Keywords: cellulose nanocrystals, modifications, polylactic acid, active packaging, antibacterial activity, compost disintegrability

1. Introduction

Foodborne diseases are global public health concerns that cause considerable socioeconomic implications. In fact, the problem is caused by consuming food contaminated with microorganisms or chemical substances that result in over 200 diseases (Gao et al., 2022). According to the estimation of the World Health Organization, foodborne diseases lead to over 420,000 deaths annually, with 40% being children under five (WHO, 2020). Among the solutions to reduce foodborne diseases, antibacterial packaging is an important approach to controlling foodborne pathogens during transportation and storage. At the same time, the increasing environmental concerns about non-degradable plastics bring awareness of "green" packaging materials. Numerous research efforts have been made to promote the applications of biodegradable polymers, which include polysaccharides, proteins of animal or plant origin, lipids, and polyesters from microbial sources (Fonseca-García et al., 2021; Omerović et al., 2021). Among them, polylactic acid (PLA) has been reported as a promising candidate to replace the fossil-based plastic, due to its renewability, biodegradability, facial processing, and biocompatibility (Ma et al., 2022; Shojaeiarani et al., 2022). PLA has the largest market share in the biodegradable plastic field, estimated for a market of $6.5 billion by 2025 (Shojaeiarani et al, 2020). Various PLA based antimicrobial packaging materials have been developed by the incorporation of functional agents such as metal oxide (Zhang et al., 2021), lignin (Cerro et al., 2021), chitosan (Kongkaoroptham et al., 2021), and essential oil (Fiore et al, 2021). For instance, Jiang et al. (Jiang et al., 2022) prepared antibacterial membranes based on PLA, polybutylene adipate terephthalate, carboxymethyl cellulose, and silver, which showed the effective antibacterial property against *Staphylococcus aureus* (*S. aureus*) and *Escherichia coli* (*E. coli*). However, the poor mechanical and barrier properties of PLA films limited their applications in food packaging due to the low crystallinity of PLA (Beauson et al., 2022; Sharafi et al., 2022).

Cellulose nanocrystals (CNCs) have received noticeable attention owing to their unique morphology, high mechanical strength, and broad functionalization capacities (Huang et al., 2020). Numerous studies focused on the reinforcing effects of CNCs on the mechanical properties of packaging films (Niinivaara et al., 2021; Rojas-Lema et al., 2021; Salmieri et al., 2014a, 2014b). To further broaden the application scope of CNCs, recent research investigated the modifications of CNCs with multifunctions and applied them as functional nanofillers of packaging materials. For example, Koshani et al. (Koshani et al., 2021) synthesized the antibacterial hairy CNCs with the conjugated photosensitizer rose bengal, which could inactivate over 80% of both *Listeria monocytogenes* and *Salmonella enterica* serotype Typhimurium upon normal light irradiation. Shin et al. (Shin et al., 2022) prepared the functionalized CNCs by grafting 3-pentadecylphenol that showed the antibacterial property of 99.99% against *E. coli*. However, these nanofillers needed to be incorporated when the packaging materials were formed, and the effects of different modified CNCs on compostable packaging have been seldom compared.

Packaging materials based on biopolymers will help reduce the negative effect on the environment, while the antibacterial property can better protect food products and decrease food waste. In this study, we hypothesized that (i) a sprayed coating of modified CNCs could improve the performance of PLA films, and (ii) the effects were related to the different modifications of CNCs. CNCs derived from waste textile were selected as a model and modified with N-halamine (methacrylamide, MAM), quaternary ammonium salt (CTAB), and metal oxide (ZnO), respectively. The modified CNCs were spray-coated on the surface of PLA films, and their effects on the properties (antibacterial activity, mechanical properties, gas barrier properties, and compost disintegrability) of PLA films were investigated. Moreover, the preservation of pork loin with CNC-coated or uncoated PLA films was monitored.

2. Materials and Methods

2.1. Materials

Waste cotton clothes were kindly provided by Renaissance (Montreal, QC, Canada). CNCs were directly extracted from textile waste by using sulfuric acid hydrolysis, according to our previous work (Huang et al., 2020). Cetyltrimethylammonium bromide (CTAB, ≥98%), zinc acetate dihydrate (>95%), sodium hydroxide (NaOH, ≥97.0%), methacrylamide (MAM, 98%), sodium persulfate (≥98%), sodium thiosulfate anhydrous (≥98%), tetrahydrofuran (THF, >95%), and glacial acetic acid (≥99.7% w/w) were purchased from Fisher Scientific (Ottawa, ON, Canada) and used without further treatment. Pellet PLA (Ingeo 4043D grade, >98%, density of 1.24 g/cc) was purchased from NatureWorks (Minnetonka, MN, USA). Luria–Bertani (LB) medium and tryptic soy agar (TSA) were purchased from Becton, Dickinson and Company (Franklin Lakes, NJ, USA), and phosphate-buffered saline (10× PBS) was obtained from VWR International (Mississauga, ON, Canada).

2.2. Modification of CNCs

MAM-modified CNCs were prepared according to the method reported by Liu et al. (Liu et al., 2017) with some modifications. The desired amount of NaOH was added into 50.00 g of CNC aqueous suspension (10 wt%), and then 5.00 g MAM and 0.03 g sodium persulfate were added and stirred at room temperature for 20 min. The reaction was conducted at 65 °C (in a water bath) for 5 hours. After that, the product was washed with distilled water to remove unreacted MAM and sodium persulfate and coded as MAM-CNCs.

The preparation of CTAB-modified CNCs was carried out according to the method described by Ranjbar et al. (Ranjbar et al., 2020). Briefly, 40.00 g of CNC aqueous suspension (5 wt%) was slowly added to 20.00 g of CTAB solution (5 wt%). The mixture was stirred at room temperature for 2 hours. Then, the modified CNCs were washed with distilled water to remove the unbounded CTAB and coded as CTAB-CNCs.

The zinc oxide-modified CNCs were synthesized by using zinc acetate as the zinc precursor and NaOH as a reducing agent, according to a previous report (Badawy et al., 2021) with some modifications. In brief, zinc acetate solution (50.00 g, 10 wt%) was mixed with CNC aqueous suspension (50.00 g, 2.5 wt%) and stirred at 80 °C for 1 hour. Then, NaOH solution (50 mL, 0.1 mol/L) was added dropwise to the mixture, and the suspension showed a milky color. The reaction continued at 80 °C for 2 hours under stirring. The obtained samples were well-washed with distilled water and coded as ZnO-CNCs.

2.3. Preparation of PLA/CNC composite films

PLA films were prepared by dissolving 0.8 g PLA pellets in 10 mL THF, and the solution was filled into a glass mold and dried at 25 °C for 12 hours. After washing with distilled water, the modified CNCs were centrifugated (7000 g, 30 min, Eppendorf centrifuge 5430, NRW, Germany), dispersed in acetic acid (2 w/v%), and then sprayed on the surface of PLA films (length × width × thickness: 8 cm × 6 cm × 0.15 mm). The PLA/CNC composite films were dried in the fume hood for 24 hours and coded as PLA-CC4, PLA-CC8, PLA-ZC4, PLA-ZC8, PLA-MC4, and PLA-MC8, corresponding to the CTAB-CNCs, ZnO-CNCs, and MAM-CNCs contents (based on the dry weight of PLA) of 4 and 8 wt%, respectively. The films were stored at 25 °C and 50% relative humidity for 3 days prior to analysis.

2.4. Characterizations

2.4.1. Fourier-transform infrared (FTIR) spectroscopy

FTIR spectra of modified CNCs and PLA/CNC composite films were obtained by using a Cary 630 FTIR spectrometer with an attenuated total reflectance sampling module (Agilent technologies, Inc., USA). The spectra were collected in the range of 4000-650 cm^{-1} as the average of 64 scans with a resolution of 2 cm^{-1}, using the empty accessory as blank.

2.4.2. X-ray diffraction (XRD)

XRD patterns of pristine and modified CNCs were obtained using an Empyrean 3 (Malvern Panalytical Ltd., UK) X-ray diffractometer in a Bragg Brentano configuration, with Cu Kα radiation between 4° and 80°. The crystallinity index (CrI) was determined by the peak height method (Park et al., 2010) in terms of Equation (1):

$$CrI\ (\%) = \frac{I_{(200)} - I_{am}}{I_{(200)}} \times 100\% \qquad \text{Equation (1)}$$

where $I_{(200)}$ is the maximum diffraction intensity associated with surface areas of crystalline cellulose, and I_{am} is the diffraction intensity of an amorphous cellulose fraction.

2.4.3. UV-vis spectroscopy

UV-vis spectra of pristine CNC and ZnO-CNC suspensions were collected on a DU 800

UV-Vis spectrophotometer (Beckman Coulter, USA) in the wavelength range of 200-400 nm against distilled water as blank.

2.4.4. Zeta potential measurement

The surface charge of CNC samples was measured using the NanoBrook Omni zeta potential analyzer (Brookhaven Instruments Corporation, USA). Triplicate measurements were taken at 25 °C after the samples were conditioned for 300 seconds.

2.4.5. Transmission electron microscopy (TEM)

The morphology of modified CNCs was observed using the Talos F200X G2 TEM (Thermo Fisher Scientific, USA). A tiny drop of diluted CNC suspension was deposited on a carbon-coated copper grid. After air drying at room temperature, the sample was imaged on TEM at a voltage of 200 kV.

2.4.6. Scanning electron microscopy (SEM)

The surface morphology of PLA/CNC composite films was observed by Hitachi TM1000 SEM (NJ, USA), operating at an acceleration voltage of 4 kV. The film samples were sputtered with 4 nm gold-platinum prior to observation and photographing.

2.4.7. Antibacterial test

Two strains were used for the antibacterial testing, namely *S. aureus* ATCC 6538 (Gram-positive) and *E. coli* K12 (Gram-negative). Each strain was prepared from -80 °C 20% glycerol stock and streaked for isolation on LB agar plates. The plates were incubated at 37 °C overnight, and isolated colonies were picked for inoculation of 4 mL LB broth at 37 °C with constant shaking. After 16 hours, a concentration of ca. 8 log for each bacterial culture was achieved, and the bacterial inoculums were prepared by diluting the culture with PBS to a certain concentration for further experiments.

The antibacterial efficacy of modified CNCs was evaluated by mixing 20 mL of CNC suspension and 200 μL of bacterial inoculum to a final concentration of 10^5 CFU/mL (Tang et al., 2020). The mixture was incubated for 1 hour with constant shaking, and then the upper suspension was used for serial dilution using PBS. After that, the diluted solution was spread onto the surface of LB agar plate and incubated at 37 °C for 24 hours. The colonies on the plate were enumerated to calculate the log reduction.

The antibacterial activity of PLA/CNC composite films against *S. aureus* and *E. coli* was analyzed by a modified AATCC 100 test method (Xu et al., 2021). The composite films with a thickness of 0.15 mm were cut into 2 cm × 2 cm. Then, 20 µL of bacterial suspension (~10^6 CFU/mL) was sandwiched between two films to enable sufficient contact. After 1 hour of contact, 4 mL of sterile sodium thiosulfate was added and vortexed to rinse off bacteria. The rinsing solution was serially diluted for the plating assay.

The zone of inhibition was measured using the disc diffusion method (Zhang et al., 2021). *S. aureus* and *E. coli* suspensions with a concentration of around 10^8 CFU/mL were evenly spread on the LB agar plates, and the composite films (diameter of 6 mm) were placed over the surface of the inoculated plate. The plates were incubated at 37 °C for 24 hours, and the bacterial inhibition zone was measured.

2.4.8. Mechanical properties

The mechanical properties of PLA/CNC composite films were tested using an eXpert 7601 single column testing machine (ADMIT, USA) at 25 °C according to the standard ASTM D882. The dimension of film specimens was 60 mm × 10 mm × 0.15 mm (length × width × thickness). The initial grip separation distance was set as 20 mm, and the separation speed was 20 mm/min. The thickness of the films was measured by a Traceable digital caliper (Fisher Scientific, ON, Canada).

2.4.9. Gas barrier properties

Water vapor permeability (WVP) was determined using a water vapor permeability tester (model 3/61, Mocon, Inc., USA) at 37 °C and 90% relative humidity (RH). WVP values were calculated using Equation (2) (Zhou et al., 2022):

$$WVP = \frac{WVTR \times n}{\Delta p} \quad \text{Equation (2)}$$

where n is the film thickness (m), and Δp is the partial pressure difference across the films (Pa).

The oxygen transmission rate (OTR) of PLA/CNC composite films was determined at 23 °C and 0% RH using an oxygen permeability tester (model 2/22, Mocon, Inc., USA).

2.4.10. Water contact angle

The water contact angle was tested by a contact angle meter (Future digital scientific, Co. USA) using the sessile drop method. The water droplet (5 μL) was placed on the film surface, and the image was immediately captured and analyzed with the goniometer at room temperature. Each measurement was performed on a different spot of the film, and the results were based on the average of three measurements.

2.4.11. Disintegration under composting conditions

The disintegration performance of PLA/CNC composite films was tested following the ISO-20200 standard (ISO, 2015). Briefly, solid synthetic waste was prepared by mixing 40% sawdust, 30% rabbit feed, 10% ripe compost, 10% corn starch, 5% saccharose, 4% corn oil, and 1% urea together. After that, the dry waste was mixed with water in 45:55 ratio. The composite films were cut into 25 mm × 25 mm and buried at 6 cm depth in the composting reactor containing reconstituted wet waste. The reactor was then put in an air-circulation oven at 58 ± 2 °C, and water was added periodically to maintain the humidity in the compost. The films were recovered from the reactor at different times (3, 7, 10, and 14 days), dried, and weighed. The weight loss of the films was calculated using Equation (3) (Cerro et al., 2021):

$$Weight\ loss\ (\%) = \frac{m_i - m_d}{m_i} \times 100\% \qquad \text{Equation (3)}$$

where m_i and m_d were the initial dry mass and residue dry mass of tested samples, respectively.

2.4.12. Meat preservation test

Pork loin was selected as a food model and purchased from a local market. The pork was cut into 1 cm × 1 cm × 1 cm portions and randomly divided into five groups. The test groups were packaged with PLA/CNC composite films, and the control groups were either unpackaged or wrapped with neat PLA films. The samples were placed on the trays and stored at 4 °C. The total viable count (TVC) values were determined at 0, 1, 3, 5, 7, and 10 days of storage according to the method reported by Zhong et al. (Zhong et al., 2021).

Briefly, the pork samples were transferred aseptically to a stomacher bag and added with PBS solution. The mixture was homogenized for 2 minutes using a lab stomacher blender (Seward, UK). Then, serial dilutions were prepared with PBS, spread on TSA plates, and incubated at 37 °C for 48 hours. The experiments were performed in triplicate, and the results of TVC were reported as CFU/g.

2.5. Statistical analysis

The experiments were carried out in triplicate, and data were presented as the mean ± standard deviation. The statistical analysis of the data was carried out through a one-way analysis of variance (ANOVA) using IBM SPSS Statistics 26 software, and the differences between means were analyzed by LSD post-hoc analysis at the confidence level of 0.05.

3. Results and Discussion

3.1. Structure of modified CNCs

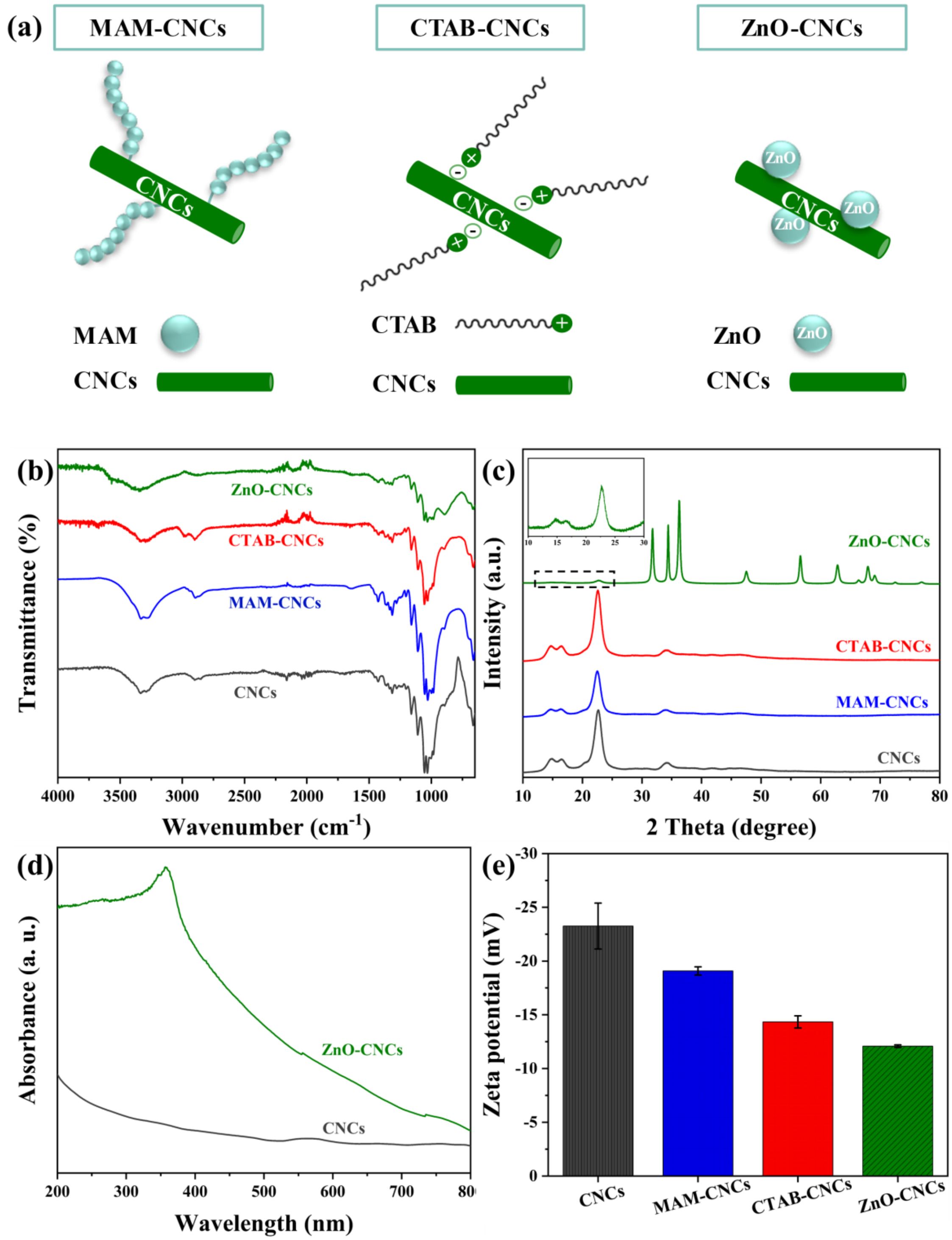

Figure 1. (a) Illustration, (b) FTIR spectra, (c) XRD patterns, (d) UV-vis spectra, and (e) zeta potential of pristine and modified CNCs.

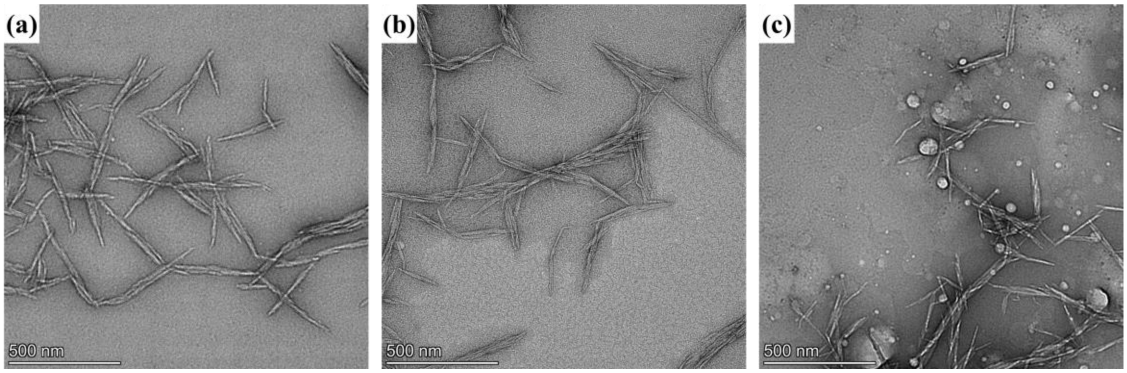

Figure 2. TEM images of (a) MAM-CNCs, (b) CTAB-CNCs, and (c) ZnO-CNCs.

Figure 1 (a) illustrates the different modified CNCs, and their chemical structures were analyzed by FTIR (Figure 1 (b)). The FTIR spectrum of unmodified CNCs showed the characteristic peaks at 3338 cm^{-1}, 2893 cm^{-1}, 1427 cm^{-1}, 1371 cm^{-1}, 1315 cm^{-1}, 1160 cm^{-1}, 1055 cm^{-1}, 1031 cm^{-1}, and 893 cm^{-1}, corresponding to O-H stretching, C-H stretching, C-H bending, CH_2 bending, O-H bending, asymmetric vibration of C-O-C, pyranose ring stretching, and β-glycoside bonds of the glucose ring, respectively. After the modification with MAM, the FTIR spectrum of MAM-CNCs showed a significant new peak at 1643 cm^{-1} assigned to amide carbonyl C=O bond. Besides, the peak at 1600 cm^{-1} attributed to C=C bond of MAM was not observed in MAM-CNCs, indicating that the residue of unreacted MAM monomer was removed from the product. Proof of the successful modification of MAM onto CNCs was interpreted in comparison with the previous report (Rosace et al., 2017). Compared to original CNCs, only slight changes of FTIR spectrum were observed for CTAB-CNCs. Strong C-H stretching at 2984 cm^{-1} and 2900 cm^{-1}, corresponding to the long-chain alkyl group of CTAB, suggested the presence of CTAB on CNCs and the absence of direct chemical bonding (Ranjbar et al., 2020). For ZnO-CNCs, no changes were found in the FTIR spectrum (Sharma et al., 2019), but a new and strong characteristic peak at 365 nm appeared in the UV-vis spectrum (Figure 1 (d)), ascribed to the basic bandgap absorption of ZnO (Xiao et al., 2020). It has been reported that hydrogen bonds and electrostatic attraction are two potential interactions between CNCs and ZnO (Fu et al., 2015; Sharma et al., 2019; Zhao et al., 2017). The XRD patterns of pristine and modified CNCs are shown in Figure 1 (c). All the samples exhibited similar diffraction peaks at 14.6° $(1\bar{1}0)$, 16.4° (110), and 22.5° (200), ascribed to cellulose I_β crystal structure (Duarte Urueña et al., 2021). ZnO-CNCs also showed the peaks at 31.8°, 34.5°, 36.2°, 47.8°, 56.5°, 62.8°, and 68.0°, corresponding to (100), (002), (101), (102), (110), (103), and (112) of the ZnO crystal structure, respectively (Elfeky et al., 2020). The surface charges of the modified CNCs are shown in Figure 1 (e). The original CNCs had a zeta potential value of around -23 mV, which was similar to the samples from sago frond wastes prepared by sulfuric acid hydrolysis (Arnata et al., 2020; Asadi et al., 2021). After surface modification, MAM-CNCs showed similar surface charges with CNCs. The electrostatic interaction between CTAB and CNCs resulted in the reduced negative charges of CNCs (Baggio et al., 2022), while ZnO-CNCs had the least charges due to the attracted ZnO (Badawy et al., 2021; Guan et al., 2019). Figure 2 shows the morphologies of modified CNCs, which had a typical rod-like shape with an average length of 158 nm and a diameter of 10 nm, without obvious aggregation (Badawy et al., 2021; Gahrooee et al., 2021; Li et al., 2020). The particle size of ZnO in Figure 2 (c) was 36±16 nm, which was similar to the reported ones (Elfeky et al., 2020; Lizundia et al., 2018).

3.2. Antibacterial activity

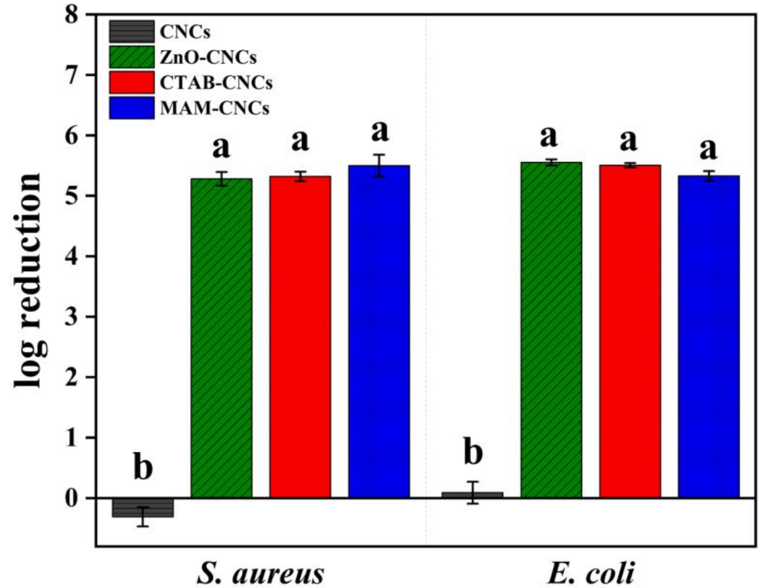

Figure 3. Antibacterial efficiency of pristine and modified CNCs against *S. aureus* and *E. coli*. Statistical significance ($p < 0.05$) between different CNC samples was indicated by different letters.

The pristine and modified CNCs were cultivated with Gram-positive (*S. aureus*) and Gram-negative (*E. coli*) bacteria to evaluate their antibacterial activity. For MAM-CNCs, chlorination treatment with sodium hydrochloride was conducted to convert the N-H bond to oxidative chlorine, which activated the antibacterial capacity of MAM-CNCs (Chang et al., 2018). In contrast, ZnO-CNCs and CTAB-CNCs did not require any pre-treatment. As shown in Figure 3, the original CNCs did not exhibit any effect against both *S. aureus* (-0.31 log) and *E. coli* (0.09 log), which was consistent with a previous report (Zhou et al., 2022). At the same time, significant antibacterial efficiency ($p < 0.05$) was observed in all modified CNC samples, with >99.999% reduction for both strains. After the chlorination treatment, MAM-CNCs could generate active chlorine that transferred to cell membranes and resulted in cell death (Kong et al., 2019). CTAB-CNCs could change the bacterial membrane permeability or bacterial surface electrostatic balance after contact, ultimately leading to cell death (Xie et al., 2011). As for ZnO-CNCs, several probable routes have been proposed to explain their bactericidal mechanism. The released ion mediated killing was one of the possible mechanisms, where the released Zn^{2+} entered the bacterial cells, leading to inhibited DNA replication. ZnO might also attach and induce deformation of the bacterial cell wall (Ahmad, 2021; Roy & Rhim, 2019; Zhang et al., 2021; Larki et al., 2022).

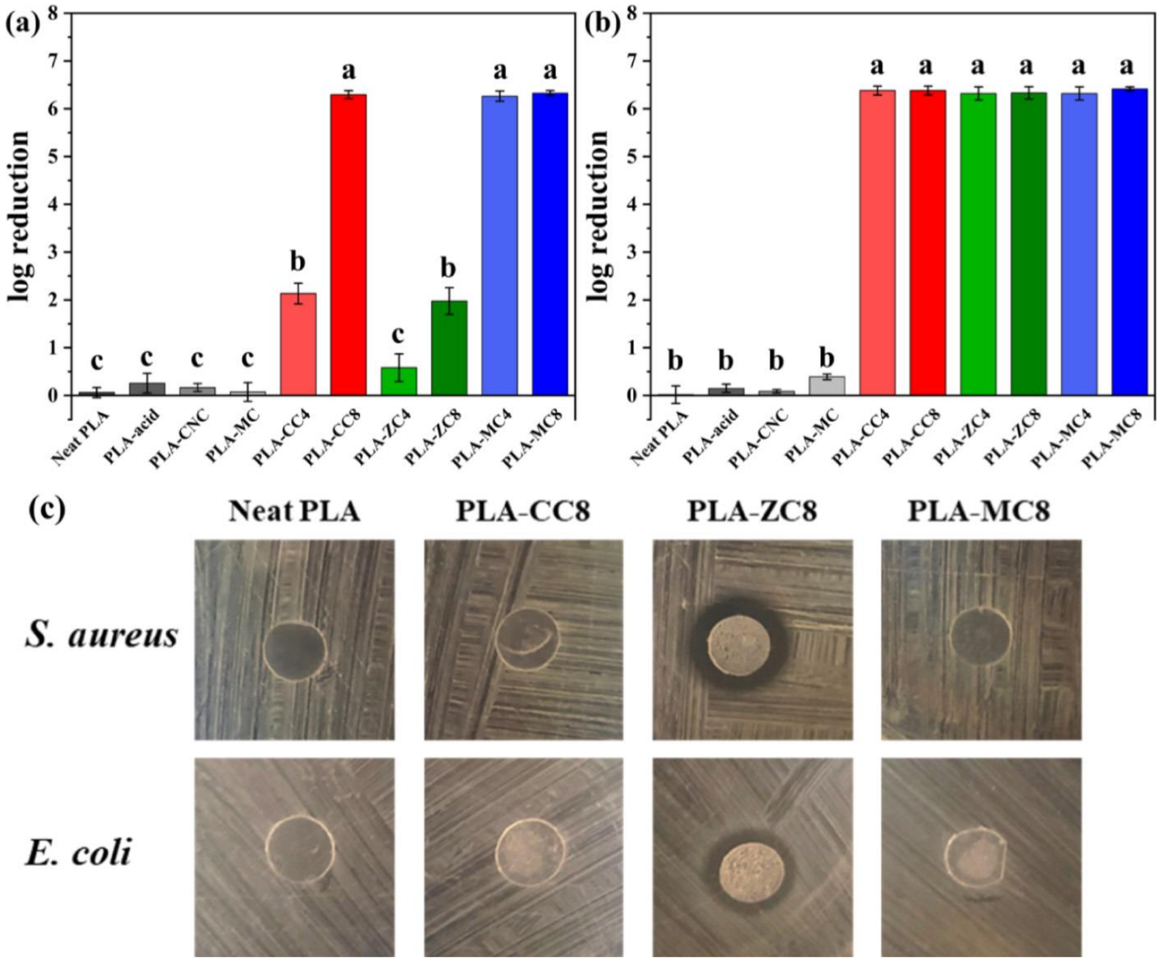

Figure 4. (a, b) Antibacterial activity and (c, d) images of inhibition zone of PLA/CNC composite films (1-Neat PLA, 2-PLA-CC8, 3-PLA-MC8, 4-PLA-ZC8) against *S. aureus* and *E. coli*. Means with different letters on the column top were significantly different ($p < 0.05$).

As shown in Figure 4 (a, b), the control groups, including neat PLA film, neat PLA films treated with acetate acid, PLA film with pristine CNC coating, and PLA film with MAM-CNC coating (without chlorination), did not show any antibacterial activity against either *S. aureus* or *E. coli*. On the contrary, all the antibacterial CNC coatings exhibited obvious effects, depending on the types of bacteria and CNC modifications, as well as the amount of CNC derivatives. Particularly, PLA-CC composite films displayed an increasing log reduction of *S. aureus* from 2.14 to 6.29 with increasing CNC contents, while PLA-MC showed high antibacterial efficiency against *S. aureus* even with low coating mass. However, the antibacterial activity of PLA-ZC for *S. aureus* was not as high as the other two coatings. In the case of *E. coli*, all three CNC coatings showed significant antibacterial efficiencies (>99.9999%) upon 1 hour of contact. It meant that CTAB-CNC and ZnO-CNC coatings had a stronger influence upon the Gram-negative bacteria than the Gram-positive strains, and the chlorinated MAM-CNCs showed excellent antibacterial activity for both types of bacteria. Similar results have reported that *E. coli* was less resistant to the antibacterial agents (e.g., ZnO nanoparticles) than the Gram-positive bacteria (Shankar et al., 2018; Zhang et al., 2017). In one aspect, the Gram-positive *S. aureus* consists of a thicker cell wall than that of the Gram-negative *E. coli*; in another aspect, the Gram-positive bacteria could form aggregates to protect the internal cells from the antibacterial agents (Pantani et al., 2013). Based on the antibacterial efficiencies, PLA-CC8, PLA-ZC8, and PLA-MC8 were selected for the following tests. The inhibition zones of neat and coated PLA films are shown in Figure 4 (c, d). No obvious inhibition zone was observed in neat PLA, PLA-CC8, and PLA-MC8 films for both *S. aureus* and *E. coli*, suggesting little or no release of the antibacterial agents from the coatings to the agar plates. On the contrary, PLA-ZC8 films exhibited similar inhibition rings (~10 mm) against *S. aureus* and *E. coli*, which was due to the release of ZnO and/or Zn^{2+} ions (Pantani et al., 2013; Wahid et al., 2019). Table 1 summarizes the antibacterial properties of the recently reported composite materials, suggesting that the sprayed coatings of modified CNCs provided a promising strategy for effective bacteria elimination.

Table 1. Antibacterial activities of recently reported composite materials.

Composite materials	Antibacterial agent	Antibacterial activity		References
		S. aureus	*E. coli*	
PLA/CNC nanofluids	CNC nanofluids	98.5%	92.7%	(Shen et al., 2021)
PLA/acetylated CNCs/ZnO	ZnO	99.9%	99.9%	(Yu et al., 2021)
PLA/propolis	Propolis	-	99.99%	(Ulloa et al., 2019)
CMC/gelatin/nano ZnO	CMC & ZnO	84.7%	99.2%	(Chen et al., 2022)
PU/chitin/ZnO-doped-SiO_2 nanoparticles	ZnO-doped-SiO_2 nanoparticles	99.289%	99.942%	(Moustafa et al., 2022)
Graphene/N-halamine-coated cotton fabrics	N-halmaine	99.9999%	99.9999%	(Xu et al., 2022)
Polycaprolactone/Zein/ZnO-QAS	ZnO-QAS nanoparticles	99.9999%	99.9999%	(Wang et al., 2021)
PU/PSDT	N-halmaine & QAS compound	99.9999%	99.9999%	(Tian et al., 2021)
PLA/ZnO-CNCs	ZnO-CNCs	99%	99.9999%	Present work
PLA/CTAB-CNCs	CTAB-CNCs	99.9999%	99.9999%	Present work
PLA/MAM-CNCs	MAM-CNCs	99.9999%	99.9999%	Present work

Note: CMC-carboxymethyl chitosan; PU-polyurethane; QAS-quaternary ammonium salts; PSDT-polystyrene grafted by 5, 5-dimethylhydantoin and trimethylamine.

3.3. Structure of PLA/CNC composite films

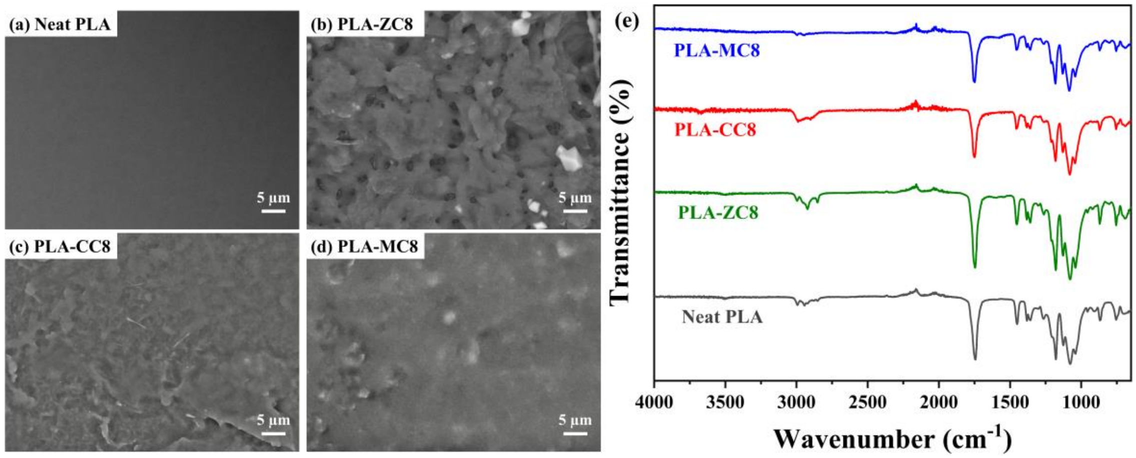

Figure 5. SEM images (a-d) and FTIR spectra (e) of neat and coated PLA films.

The surface morphology of neat and coated PLA films was observed by SEM. Figure 5 (a) displays the smooth and homogeneous surface of neat PLA without cracks or holes. The addition of coating solutions (acetic acid) resulted in the eroded surfaces, and the modified CNCs were combined with the polymeric matrix. It explained the little or no release of CNCs from the films to the agar plates. FTIR analysis of the composite films was carried out to study the molecular structures. As shown in Figure 5, the peaks of neat PLA film at 2994 cm^{-1} and 2943 cm^{-1} were associated with the C-H asymmetric and symmetric stretching in $-CH_3$ groups. The peak at 1743 cm^{-1} corresponded to the C=O stretching vibration of the ester groups. The peaks between 1450 cm^{-1} and 1357 cm^{-1} represented asymmetric and symmetric bending of C-H bond in the methyl groups, while the peaks at 1178 cm^{-1} and 1077 cm^{-1} were related to the C-O-C symmetric and asymmetric stretching (Doganay et al., 2016). With the addition of CNC coatings, no new characteristic peaks or obvious shift of peaks were observed. It indicated that no new covalent bonds were formed after the incorporation of modified CNCs.

3.4. Mechanical and barrier properties of PLA/CNC composite films

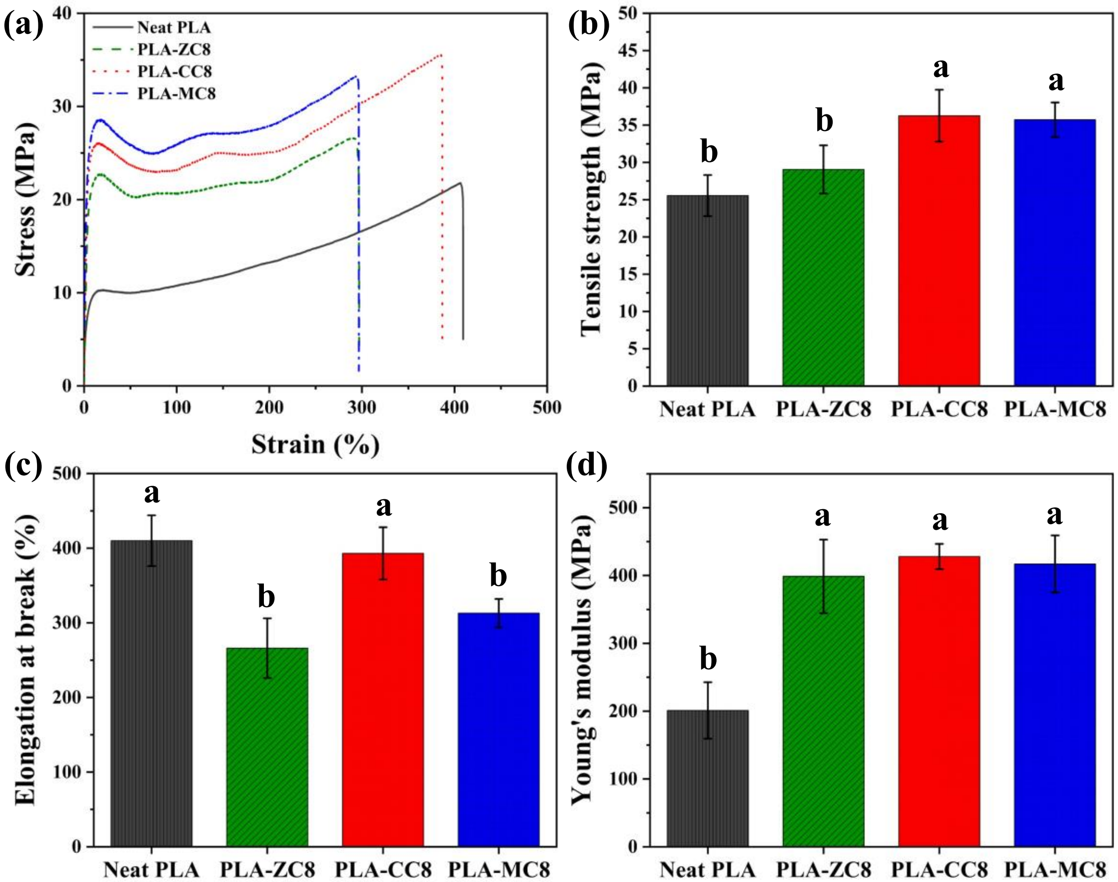

Figure 6. (a) Stress-stain curves, (b) tensile strength, (c) elongation at break, and (d) Young's modulus of neat and coated PLA films. Means with different letters on the column top were significantly different ($p < 0.05$).

Mechanical properties of neat and coated PLA films were measured, and the representative stress-strain curves are shown in Figure 6 (a). Their thicknesses did not have any significant difference, and all the films exhibited similar curves, beginning with elastic deformation and following by plastic deformation. Obvious yielding points were observed, which define the limitation of the elastic behavior and the beginning of the plastic behavior (Beauson et al., 2022). For the neat PLA films, the stress at the yielding point was ~10 MPa and the films fractured at the strain of ~400%. For all types of coated PLA films, an increase in yield strength was clearly observed (20-30 MPa), suggesting their improved resistance to loading before permanent deformation (Aghajani et al., 2018). Figure 6 (b-d) shows the variations of tensile strength, elongation at break, and Young's modulus of PLA films with different CNC coatings. All the coatings significantly increased the Young's modulus, and PLA-CC8 and PLA-MC8 had an improved tensile strength, but only PLA-CC8 could maintain the ductility of the neat PLA films. The increase in mechanical strength could be explained that the surface coating well combined with the polymeric matrix and acted as a scaffold (Gulzar et al., 2022). The retained ductility of PLA-CC8 might be attributed to the good interfacial compatibility, which contributed to effective stress transfer and delaying the stretching failure (Dehnad et al., 2014; Jin et al., 2020).

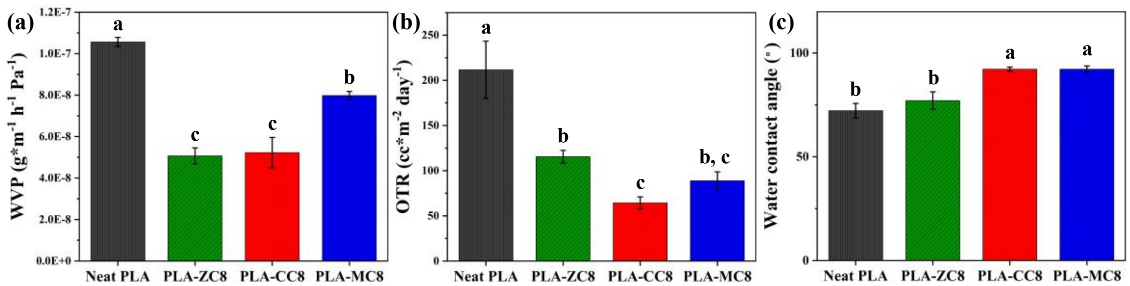

Figure 7. (a) WVP, (b) OTR, and (c) water contact angle of neat and coated PLA films. Means with different letters on the top of the columns were significantly different ($p < 0.05$).

The water vapor and oxygen barrier properties of neat and coated PLA films are important to their potential applications in packaging. As shown in Figure 7 (a, b), the neat PLA film had an average WVP value of 1.06×10^{-7} g m^{-1}h^{-1}Pa^{-1} and OTR value of 211.72 cc m^{-2}day^{-1}, while the permeability of PLA/CNC composite films significantly ($p < 0.05$) decreased. Particularly, PLA-CC8 showed the lowest WVP and OTR values of 5.22×10^{-8} g m^{-1}h^{-1}Pa^{-1}and 64.34 cc m^{-2}day^{-1}, respectively. It was because the modified CNCs tightly combined with PLA after solution coating and formed a dense layer on the surface of the films (Zhou et al., 2021). These values were relatively lower than those reported previously; for example, the WVP value of PLA/ZnO composite films was around 7×10^{-8} g m^{-1}h^{-1}Pa^{-1} (Shankar et al., 2018), and the poly(ethylene furanoate)/PLA films had an OTR value of 144 cc m^{-2}day^{-1} (Fredi et al., 2022). Figure 7 (c) shows the water contact angle of neat and coated PLA films. As expected, the neat PLA film had a hydrophilic surface with a contact angle of around 74.2° (Vilarinho et al., 2021). A slight increase ($p > 0.05$) in contact angle of PLA-ZC8 was observed, which might be due to the hydrophobic nature of ZnO (Roy & Rhim, 2019). The surface hydrophobicity of PLA-CC8 and PLA-MC8 films was significantly higher than that of the neat PLA film. It could be explained by the existence of long carbon chains on the modified CNCs (Ly & Mekonnen, 2020).

3.5. Compost disintegrability

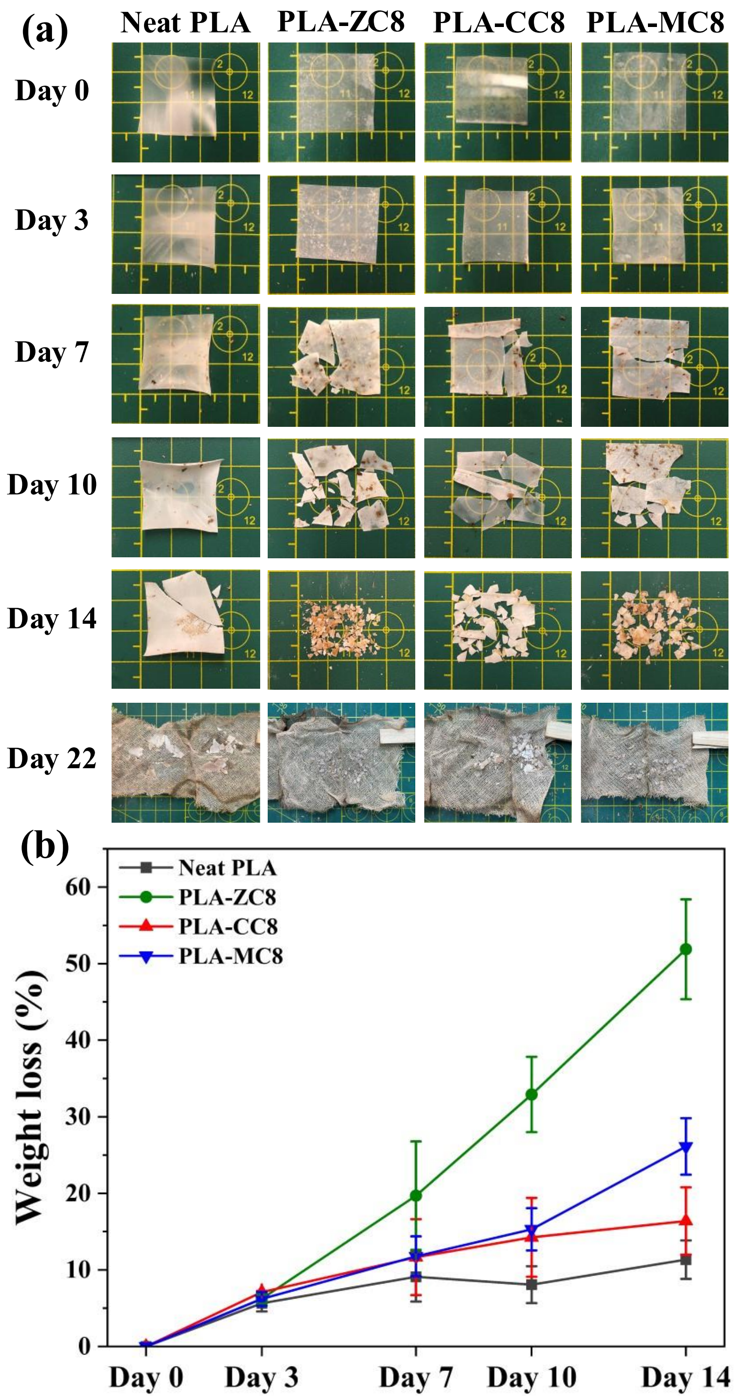

Figure 8. (a) Photos and (b) weight loss of neat and coated PLA films after incubating under composting conditions.

PLA films hold great potential for "green" packaging materials because of their degradable character under specific conditions (Rojas et al., 2021). In this regard, the effect of CNC coatings on the disintegrability of PLA films under composting conditions was investigated. As shown in Figure 8 (a), no particular alterations were observed after 3 days for all the samples. The PLA/CNC composite films became opaque, and the fragmentation started after 7 days. Compared to neat PLA film, the fragmentation of CNC coated PLA films was more obvious on day 10 and day 14. The weight loss showed a similar trend (Figure 8 (b)). All the films exhibited a gradual increase in weight loss under composting conditions. Especially after 14 days, the weight loss of PLA-ZC8, PLA-MC8, and PLA-CC8 films was about 51.88%, 26.12%, and 16.38%, respectively, against 11.34% for the neat PLA film. To be noted, only a few tiny fragments were recovered on day 22, so it was difficult to weigh and calculate the weight loss. The results revealed a faster disintegration rate of PLA/CNC composite films, and it was consistent with reported results that CNCs acted as a source of energy and carbon and facilitated the initiation of disintegration (Degli-Innocenti, 2021; Lizundia et al., 2018; Sun et al., 2022).

3.6. Preservation of pork

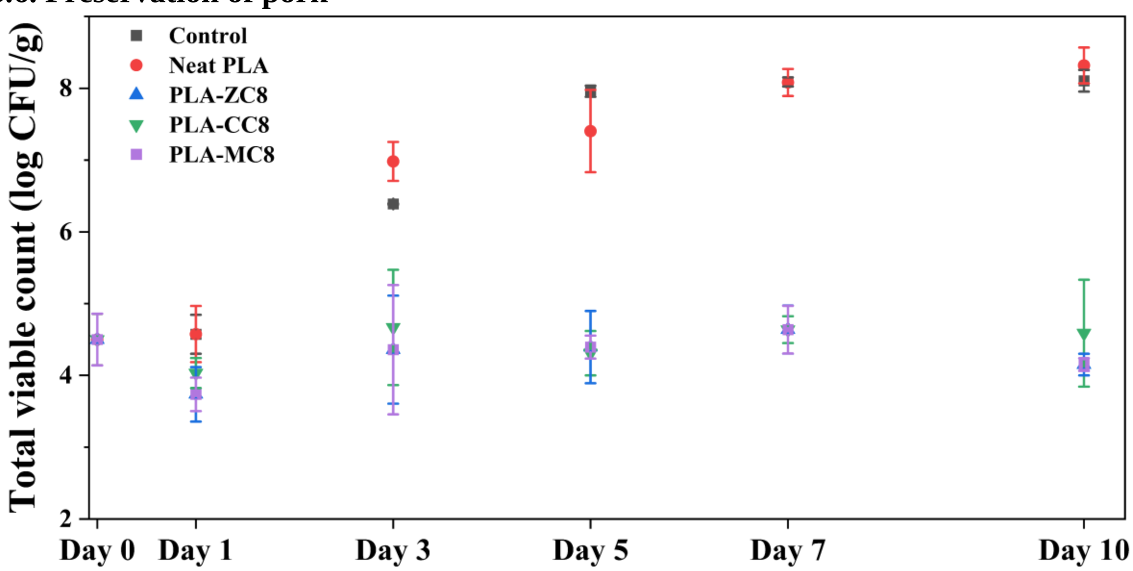

Figure 9. Total viable counts of pork samples during storage at 4 °C.

Pork is a commonly consumed red meat worldwide, containing rich sources of certain protein, vitamins, and minerals. However, cross-contamination happens frequently during the production. Herein, pork was chosen as a model for evaluating the packaging performance. The initial TVC value of 4.50 log CFU/g in the raw pork was similar to a reported value (Vargas Romero et al., 2021). As shown in Figure 9, the total viable population of the microorganism in pork samples (unpackaged and wrapped with neat PLA film) rapidly increased during the storage period. The permissible limit of the overall microorganism in fresh meat should be less than 5×10^6 CFU/g, as regulated by European Commission No. 2073/2005 (Commission, 2005). Therefore, both the control sample and neat PLA group exceeded the limit after 3 days of cold storage (about 6.39 and 6.98 log CFU/g). It was worth noting that all PLA/CNC composite film wrapped pork samples had delayed bacteria growth, and their TVC values were lower than 5×10^6 CFU/g after storage at 4 °C for 10 days. No significant difference was observed among the three coatings, which indicated the sufficient antibacterial activity of all these modified CNCs for extended shelf life of fresh pork.

4. Conclusions

This work demonstrated a convenient method to fabricate compostable packaging films with antibacterial activity. The effects of sprayed coatings of three types of modified CNCs (CTAB-CNCs, ZnO-CNCs, and MAM-CNCs) on the structure and properties of PLA films were revealed. Especially, ZnO-CNC coated PLA films exhibited prominent disintegration behavior. After incubating under composting conditions for 14 days, a weight loss of 51.88% was recorded, which was over 5 times higher than the neat PLA film. CTAB-CNC coating significantly increased the tensile strength and Young's modulus without affecting the ductility, and at the same time, showed the improvement of 51% and 70% in water vapor and oxygen barrier properties, respectively. MAM-CNC coated PLA films had the most effective antibacterial capacity against both Gram-positive and Gram-negative bacteria. With a small amount of coating, PLA-MC4 films could inactivate >99.9999% of *S. aureus* and *E. coli* upon 1 hour of contact. After all, three PLA/CNC composite films could significantly extend the shelf life of wrapped pork from 3 days to more than 10 days. Further investigations are expected to ensure that the biocompatibility inherent to PLA films is retained after coating. Hopefully, this strategy of spray coating with modified CNCs could be applied in other plastic and paper-based packaging materials.

Author Contributions: Conceptualization, investigation, and writing, S.H.; Data collection, S.Z.; writing-review & editing and supervision, Y.W.. All authors have read and agreed to the published version of the manuscript.

Acknowledgment: We would like to acknowledge financial support from the Natural Sciences and Engineering Research Council of Canada (NSERC RGPIN-2019-04498), Natural Sciences and Engineering Research Council of Canada Discovery Launch Supplement (NSERC DGECR-2019-00472), and Canada Foundation for Innovation (39173). We would like to acknowledge McGill University ECP3 Multi-Scale Imaging Facility for the image acquisition. S.H. would like to thank the China Scholarship Council (CSC NO. 201908880002) for financial support of her Ph.D. program.

Conflicts of Interest: The authors declare no conflict of interest.

5. References

Aghajani, M., Wang, M., Cox, L. M., Killgore, J. P., Greenberg, A. R., & Ding, Y. (2018). Influence of support-layer deformation on the intrinsic resistance of thin film composite membranes. *Journal of Membrane Science, 567*, 49-57. https://doi.org/10.101 6/j.memsci.2018.09.031

Ahmad, H. (2021). Celluloses as support materials for antibacterial agents: a review. *Cellulose, 28*(5), 2715-2761. https://doi.org/10.1007/s10570-021-03703-2

Arnata, I. W., Suprihatin, S., Fahma, F., Richana, N., & Sunarti, T. C. (2020). Cationic modification of nanocrystalline cellulose from sago fronds. *Cellulose, 27*(6), 3121-3141. https://doi.org/10.1007/s10570-019-02955-3

Asadi, H., Ghalei, S., Handa, H., & Ramasamy, R. P. (2021). Cellulose nanocrystal reinforced silk fibroin coating for enhanced corrosion protection and biocompatibility of Mg-based alloys for orthopedic implant applications. *Progress in Organic Coatings, 161*, 106525. https://doi.org/10.1016/j.porgcoat.2021.106525

Badawy, A. A., Ghanem, A. F., Yassin, M. A., Youssef, A. M., & Rehim, M. H. A. (2021). Utilization and Characterization of Cellulose Nanocrystals Decorated with Silver and Zinc Oxide Nanoparticles for Removal of Lead Ion from Wastewater. *Environmental Nanotechnology, Monitoring & Management*, *16*, 100501. https://doi.org/10.101 6/j.enmm.2021.100501

Baggio, G. M., Camani, P. H., & Rosa, D. S. (2022). Concentration and carbon chain length effects of cationic surfactant in enzymatic production of cellulose nanostructures. *Journal of Molecular Liquids, 346*, 118231. https://doi.org/10.1016/j.molliq.2021.118231

Beauson, J., Schillani, G., Van der Schueren, L., & Goutianos, S. (2022). The effect of processing conditions and polymer crystallinity on the mechanical properties of unidirectional self-reinforced PLA composites. *Composites Part A: Applied Science and Manufacturing, 152*, 106668. https://doi.org/10.1016/j.compositesa.2021.106668

Cerro, D., Bustos, G., Villegas, C., Buendia, N., Truffa, G., Godoy, M. P., Rodriguez, F., Rojas, A., Galotto, M.J., Constandil, L., & Torres, A. (2021). Effect of supercritical incorporation of cinnamaldehyde on physical-chemical properties, disintegration and toxicity studies of PLA/lignin nanocomposites. *International Journal of Biological Macromolecules, 167*, 255-266.

https://doi.org/10.1016/j.ijbiomac.2020.11.140

Chang, D., Li, Z., Wang, X., Zhu, C., Dong, A., & Gao, G. (2018). N-Halamine polymer from bipolymer to amphiphilic terpolymer with enhancement in antibacterial activity. *Colloids and Surfaces B: Biointerfaces, 163*, 402-411. https://doi.org/10.1016/j.colsurfb.20 18.01.013

Chen, J., Luo, L., Cen, C., Liu, Y., Li, H., & Wang, Y. (2022). The nano antibacterial composite film carboxymethyl chitosan/gelatin/nano ZnO improves the mechanical strength of food packaging. *International Journal of Biological Macromolecules, 220*, 462-471. https://doi.org/10.1016/j.ijbiomac.2022.08.005

Commission Regulation (EC) No 2073/2005 of 15 November 2005 on microbiological criteria for foodstuffs. (2005). https://eur-lex.europa.eu/legal-content/EN/ALL/?uri=CELEX%3 A32005R2073

Degli-Innocenti, F. (2021). Is composting of packaging real recycling? *Waste Management, 130*, 61-64. https://doi.org/10.1016/j.wasman.2021.05.017

Dehnad, D., Emam-Djomeh, Z., Mirzaei, H., Jafari, S.-M., & Dadashi, S. (2014). Optimization of physical and mechanical properties for chitosan–nanocellulose biocomposites. *Carbohydrate Polymers, 105*, 222-228. https://doi.org/10.1016/j.carbpol.2014.01.094

Doganay, D., Coskun, S., Kaynak, C., & Unalan, H. E. (2016). Electrical, mechanical and thermal properties of aligned silver nanowire/polylactide nanocomposite films. *Composites Part B: Engineering, 99*, 288-296. https://doi.org/10.1016/j.com positesb.2016.06.044

Duarte Urueña, G., Ribeiro, K. C., Prestes, E., Pinheiro, L. A., & Carvalho, B. M. (2021). Extraction of Cellulose Nanocrystal from Multilayer Packaging Residues Composed of a Mixture of Eucalyptus and Pine Fibers. *Waste and Biomass Valorization, 12*(10), 5763-5777. https://doi.org/10.1007/s12649-021-01383-4

Elfeky, A. S., Salem, S. S., Elzaref, A. S., Owda, M. E., Eladawy, H. A., Saeed, A. M., Awad, M.A., Abou-Zeid, R.E., & Fouda, A. (2020). Multifunctional cellulose nanocrystal /metal oxide hybrid, photo-degradation, antibacterial and larvicidal activities. *Carbohydrate Polymers, 230*, 115711. https://doi.org/10.1016/j.car bpol.2019.115711

Fiore, A., Park, S., Volpe, S., Torrieri, E., & Masi, P. (2021). Active packaging based on PLA and chitosan-caseinate enriched rosemary essential oil coating for fresh minced chicken breast application. *Food*

Packaging and Shelf Life, 29, 100708. https://doi.org/10.10 16/j.fpsl.2021.100708

Fonseca-García, A., Jiménez-Regalado, E. J., & Aguirre-Loredo, R. Y. (2021). Preparation of a novel biodegradable packaging film based on corn starch-chitosan and poloxamers. *Carbohydrate Polymers*, *251*, 117009. https://doi.org/10.1016/j.carbpol.20 20.117009

Fredi, G., Dorigato, A., Dussin, A., Xanthopoulou, E., Bikiaris, D.N., Botta, L., Fiore, V. and Pegoretti, A. (2022). Compatibilization of Polylactide/Poly (ethylene 2, 5-furanoate)(PLA/PEF) Blends for Sustainable and Bioderived Packaging. *Molecules, 27*(19), 6371. https://doi.org/10.3390/molecules27196371

Fu, F., Li, L., Liu, L., Cai, J., Zhang, Y., Zhou, J., & Zhang, L. (2015). Construction of Cellulose Based ZnO Nanocomposite Films with Antibacterial Properties through One-Step Coagulation. *ACS Applied Materials & Interfaces, 7*(4), 2597-2606. https://doi.org/10.10 21/am507639b

Gahrooee, T. R., Abbasi Moud, A., Danesh, M., & Hatzikiriakos, S. G. (2021). Rheological characterization of CNC-CTAB network below and above critical micelle concentration (CMC). *Carbohydrate Polymers, 257*, 117552. https://doi.org/10.1016/j.carbpol.2020.117552

Gao, P., Cha, R., Luo, H., Xu, Y., Zhang, P., Han, L., Wang, X., Zhang, Z., & Jiang, X. (2022). Development of antimicrobial oxidized cellulose film for active food packaging. *Carbohydrate Polymers*, *278*, 118922. https://doi.org/10.1016/j.carbpol.202 1.118922

Guan, Y., Yu, H.-Y., Abdalkarim, S. Y. H., Wang, C., Tang, F., Marek, J., Chen, W.L., Militky, J., & Yao, J.-M. (2019). Green one-step synthesis of ZnO/cellulose nanocrystal hybrids with modulated morphologies and superfast absorption of cationic dyes. *International Journal of Biological Macromolecules, 132*, 51-62. https://doi.org/10.1016/j.ijbiomac.20 19.03.104

Gulzar, S., Tagrida, M., Nilsuwan, K., Prodpran, T., & Benjakul, S. (2022). Electrospinning of gelatin/chitosan nanofibers incorporated with tannic acid and chitooligosaccharides on polylactic acid film: Characteristics and bioactivities. *Food Hydrocolloids, 133*, 107916. https://doi.org/10.1016/j.foodhyd.2022.107916

Huang, S., Liu, X., Chang, C., & Wang, Y. (2020). Recent developments and prospective food-related applications of cellulose nanocrystals: a review. *Cellulose, 27*(6), 2991-3011. https://doi.org/10.1007/s10570-020-02984-3

Huang, S., Tao, R., Ismail, A., & Wang, Y. (2020). Cellulose Nanocrystals Derived from Textile Waste through Acid Hydrolysis and Oxidation as Reinforcing Agent of Soy Protein Film. *Polymers, 12*(4), 958. https://doi.org/10.3390/polym12040958

International Organization for Standardization. (2015). *Plastics-Determination of the degree of disintegration of plastic materials under simulated composting conditions in a laboratory-scale test* (ISO 20200:2015). https://www.iso.org/standard/63 367.html

Jiang, S., Li, Q., Wang, F., Wang, Z., Cao, X., Shen, X., & Yao, Z. (2022). Highly effective and sustainable antibacterial membranes synthesized using biodegradable polymers. *Chemosphere, 291*, 133106. https://doi.org/10.1016/j.chemosphere.2021.133106

Jin, K., Tang, Y., Zhu, X., & Zhou, Y. (2020). Polylactic acid based biocomposite films reinforced with silanized nanocrystalline cellulose. *International Journal of Biological Macromolecules, 162*, 1109-1117. https://doi.org/10.1016/j.ijbiomac.2020.06.201

Kong, X., Zhang, S., Wang, Y., Liu, Y., Li, R., Ren, X., & Huang, T.-S. (2019). Antibacterial polyvinyl alcohol films incorporated with N-halamine grafted oxidized microcrystalline cellulose. *Composites Communications, 15*, 25-29. https://doi.org/10.1016/j.coco.2019.0 6.005

Kongkaoroptham, P., Piroonpan, T., & Pasanphan, W. (2021). Chitosan nanoparticles based on their derivatives as antioxidant and antibacterial additives for active bioplastic packaging. *Carbohydrate Polymers*, *257*, 117610. https://doi.org/10.1016/j.carbpol.20 20.117610

Koshani, R., Zhang, J., van de Ven, T. G. M., Lu, X., & Wang, Y. (2021). Modified Hairy Nanocrystalline Cellulose as Photobactericidal Nanofillers for Food Packaging Application. *ACS Sustainable Chemistry & Engineering, 9*(31), 10513-10523. https://doi.org/10.10 21/acssuschemeng.1c02289

Larki, M., Enayati, M. H., & Rostamabadi, H. (2022). Basil seed gum promotes the electrospinnability of WPI for co-encapsulation of ZnO nanoparticles and curcumin. *Carbohydrate Polymers*, *296*, 119966. https://doi.org/10.1016/j.carbpol.2022.119966

Li, M.-C., Wu, Q., Han, J., Mei, C., Lei, T., Lee, S.-y., & Gwon, J. (2020). Overcoming Salt Contamination of Bentonite Water-Based Drilling Fluids with Blended Dual-Functionalized Cellulose Nanocrystals. *ACS Sustainable Chemistry & Engineering, 8*(31), 11569-11578. https://doi.org/10.1021/acssuschemeng.0c02774

Liu, Y., Li, L., Pan, N., Wang, Y., Ren, X., Xie, Z., Buschle-Diller, G., & Huang, T.-S. (2017). Antibacterial cellulose acetate films incorporated with N-halamine-modified nano-crystalline cellulose particles. *Polymers for Advanced Technologies, 28*(4), 463-469. https://doi.org/10.1002/pat.3906

Lizundia, E., Goikuria, U., Vilas, J. L., Cristofaro, F., Bruni, G., Fortunati, E., Armentano, I., Visai, L., & Torre, L. (2018). Metal Nanoparticles Embedded in Cellulose Nanocrystal Based Films: Material Properties and Post-use Analysis. *Biomacromolecules, 19*(7), 2618-2628. https://doi.org/10.1021/acs.biomac.8b00243

Ly, M., & Mekonnen, T. H. (2020). Cationic surfactant modified cellulose nanocrystals for corrosion protective nanocomposite surface coatings. *Journal of Industrial and Engineering Chemistry, 83*, 409-420. https://doi.org/10.1016/j.jiec.2019.12.014

Ma, X., Wu, N., Liu, P., & Cui, H. (2022). Fabrication of highly efficient phenylphosphorylated chitosan bio-based flame retardants for flammable PLA biomaterial. *Carbohydrate Polymers*, *287*, 119317. https://doi.org/10.1016/j.carbpol.2022.119317

Moustafa, H., Darwish, N. A., & Youssef, A. M. (2022). Rational formulations of sustainable polyurethane/chitin/rosin composites reinforced with ZnO-doped-SiO_2 nanoparticles for green packaging applications. *Food Chemistry, 371*, 131193. https://doi.org/10.1016/j.foodchem.2021.131193

Niinivaara, E., Desmaisons, J., Dufresne, A., Bras, J., & Cranston, E. D. (2021). Thick Polyvinyl Alcohol Films Reinforced with Cellulose Nanocrystals for Coating Applications. *ACS Applied Nano Materials*. https://doi.org/10.1021/acsanm.1c01244

Omerović, N., Djisalov, M., Živojević, K., Mladenović, M., Vunduk, J., Milenković, I., Gadjanski, I., & Vidić, J. (2021). Antimicrobial nanoparticles and biodegradable polymer composites for active food packaging applications. *Comprehensive Reviews in Food Science and Food Safety, 20*(3), 2428-2454. https://doi.org/10.1111/1541-4337.12727

Pantani, R., Gorrasi, G., Vigliotta, G., Murariu, M., & Dubois, P. (2013). PLA-ZnO nanocomposite films: Water vapor barrier properties and specific end-use characteristics. *European Polymer Journal, 49*(11), 3471-3482. https://doi.org/10.1016/j.eurpolymj.20 13.08.005

Park, S., Baker, J. O., Himmel, M. E., Parilla, P. A., & Johnson, D. K. (2010). Cellulose crystallinity index: measurement techniques and their impact on interpreting cellulase performance. *Biotechnol Biofuels, 3*(1),

10. https://doi.org/10.1186/1754-6834-3-10

Ranjbar, D., Raeiszadeh, M., Lewis, L., MacLachlan, M. J., & Hatzikiriakos, S. G. (2020). Adsorptive removal of Congo red by surfactant modified cellulose nanocrystals: a kinetic, equilibrium, and mechanistic investigation. *Cellulose, 27*(6), 3211-3232. https://doi.org/1 0.1007/s10570-020-03021-z

Rojas-Lema, S., Nilsson, K., Trifol, J., Langton, M., Gomez-Caturla, J., Balart, R., Garcia-Garcia, D. and Moriana, R. (2021). Faba bean protein films reinforced with cellulose nanocrystals as edible food packaging material. *Food Hydrocolloids, 121*, 107019. https://doi.org/10.1016/j.foodhyd.2021.107019

Rojas, A., Velásquez, E., Patiño Vidal, C., Guarda, A., Galotto, M. J., & López de Dicastillo, C. (2021). Active PLA Packaging Films: Effect of Processing and the Addition of Natural Antimicrobials and Antioxidants on Physical Properties, Release Kinetics, and Compostability. *Antioxidants, 10*(12), 1976. https://doi.org/10.3390/antiox10121976

Rosace, G., Colleoni, C., Trovato, V., Iacono, G., & Malucelli, G. (2017). Vinylphosphonic acid/methacrylamide system as a durable intumescent flame retardant for cotton fabric. *Cellulose, 24*(7), 3095-3108. https://doi.org/10.1007/s10570-017-1294-x

Roy, S., & Rhim, J.-W. (2019). Carrageenan-based antimicrobial bionanocomposite films incorporated with ZnO nanoparticles stabilized by melanin. *Food Hydrocolloids, 90*, 500-507. https://doi.org/10.1016/j.foodhyd.2018.12.056

Salmieri, S., Islam, F., Khan, R.A., Hossain, F.M., Ibrahim, H.M., Miao, C., Hamad, W.Y. and Lacroix, M. (2014a). Antimicrobial nanocomposite films made of poly(lactic acid)-cellulose nanocrystals (PLA-CNC) in food applications: part A—effect of nisin release on the inactivation of Listeria monocytogenes in ham. *Cellulose, 21*(3), 1837-1850. https://doi.org/10.1007/s10570-014-0230-6

Salmieri, S., Islam, F., Khan, R.A., Hossain, F.M., Ibrahim, H.M., Miao, C., Hamad, W.Y. and Lacroix, M. (2014b). Antimicrobial nanocomposite films made of poly(lactic acid)–cellulose nanocrystals (PLA–CNC) in food applications—part B: effect of oregano essential oil release on the inactivation of Listeria monocytogenes in mixed vegetables. *Cellulose, 21*(6), 4271-4285. https://doi.org/10.1007/s10570-014-0406-0

Shankar, S., Wang, L.-F., & Rhim, J.-W. (2018). Incorporation of zinc oxide nanoparticles improved the mechanical, water vapor barrier, UV-light barrier, and antibacterial properties of PLA-based nanocomposite films. *Materials Science and Engineering: C, 93*, 289-298. https://doi.org/10.1016/j.msec.2018.08.002

Sharafi Zamir, S., Fathi, B., Ajji, A., Robert, M., & Elkoun, S. (2022). Crystallinity and Gas Permeability of Poly (Lactic Acid)/Starch Nanocrystal Nanocomposite. *Polymers, 14*(14), 2802. https://doi.org/10.3390/polym14142802

Sharma, P. R., Sharma, S. K., Antoine, R., & Hsiao, B. S. (2019). Efficient Removal of Arsenic Using Zinc Oxide Nanocrystal-Decorated Regenerated Microfibrillated Cellulose Scaffolds. *ACS Sustainable Chemistry & Engineering, 7*(6), 6140-6151. https://doi.org/1 0.1021/acssuschemeng.8b06356

Shen, H., Li, Y., Yao, W., Yang, S., Yang, L., Pan, F., Chen, Z., & Yin, X. (2021). Solvent-free cellulose nanocrystal fluids for simultaneous enhancement of mechanical properties, thermal conductivity, moisture permeability and antibacterial properties of polylactic acid fibrous membrane. C*omposites Part B: Engineering*, *222*, 109042. https://doi.org/10.1016/j.compositesb.2021.109042

Shin, H., Kim, S., Kim, J., Kong, S., Lee, Y., & Lee, J.-C. (2022). Preparation of 3-pentadecylphenol-modified cellulose nanocrystal and its application as a filler to polypropylene nanocomposites having improved antibacterial and mechanical properties. *Journal of Applied Polymer Science, 139*(13), 51848. https://doi.org/10.1002/app.51848

Shojaeiarani, J., Bajwa, D. S., Stark, N. M., Bergholz, T. M., & Kraft, A. L. (2020). Spin coating method improved the performance characteristics of films obtained from poly(lactic acid) and cellulose nanocrystals. *Sustainable Materials and Technologies, 26*, e00212. https://doi.org/10.1016/j.susmat.2020.e00212

Shojaeiarani, J., Shirzadifar, A., Shine, C., & Reisi, A. M. (2022). Hybrid nanocomposite packaging films from cellulose nanocrystals, zinc sulfide quantum dots reinforced polylactic acid with fluorescent and antibacterial properties. *Polymer Engineering & Science, 62*, 1562-1570.https://doi.org/10.1002/pen.25944

Sun, C., Li, C., Li, H., Liu, M., Zheng, H., Tan, H., Wang, Y., & Zhang, Y. (2022). Modified Cellulose Nanocrystals Enhanced the Compatibility Between PLA and PBAT to Prepare a Multifunctional Composite Film. *Journal of Polymers and the Environment, 30*, 3139–3149. https://doi.org/10.1007/s10924-022-02422-4

Tang, X., Xu, H., Shi, Y., Wu, M., Tian, H., & Liang, J. (2020). Porous antimicrobial starch particles containing N-halamine functional groups. *Carbohydrate Polymers, 229*, 115546. https://doi.org/10.1016/j.carbpol.2019.115546

Tian, C., Wu, F., Jiao, W., Liu, X., Yin, X., Si, Y., Yu, J., & Ding, B. (2021). Antibacterial and antiviral N-halamine nanofibrous membranes with nanonet structure for bioprotective applications. *Composites Communications, 24*, 100668. https://doi.org/10.1016/j.coco.2021.100668

Ulloa, P. A., Vidal, J., Lopéz de Dicastillo, C., Rodriguez, F., Guarda, A., Cruz, R. M. S., & Galotto, M. J. (2019). Development of poly(lactic acid) films with propolis as a source of active compounds: Biodegradability, physical, and functional properties. *Journal of Applied Polymer Science*, *136*(8), 47090. https://doi.org/10.1002/app.47090

Vargas Romero, E., Lim, L. T., Suarez Mahecha, H., & Bohrer, B. M. (2021). The Effect of Electrospun Polycaprolactone Nonwovens Containing Chitosan and Propolis Extracts on Fresh Pork Packaged in Linear Low-Density Polyethylene Films. *Foods, 10*(5), 1110. https://doi.org/10.3390/foods10051110

Vilarinho, F., Stanzione, M., Buonocore, G. G., Barbosa-Pereira, L., Sendón, R., Vaz, M. F., & Sanches Silva, A. (2021). Green tea extract and nanocellulose embedded into polylactic acid film: Properties and efficiency on retarding the lipid oxidation of a model fatty food. *Food Packaging and Shelf Life, 27*, 100609. https://doi.org/1 0.1016/j.fpsl.2020.100609

Wahid, F., Duan, Y. X., Hu, X. H., Chu, L. Q., Jia, S. R., Cui, J. D., & Zhong, C. (2019). A facile construction of bacterial cellulose/ZnO nanocomposite films and their photocatalytic and antibacterial properties. *International Journal of Biological Macromolecules, 132*, 692-700. https://doi.org/10.1016/j.ijbiomac.2019.03.240

Wang, Y., Ying, M., Zhang, M., Ren, X., & Kim, I. S. (2021). Development of Antibacterial and Hemostatic PCL/Zein/ZnO-Quaternary Ammonium Salts NPs Composite Mats as Wound Dressings. *Macromolecular Materials and Engineering*, *306*(12), 2100587. https://doi.org/10.1002/mame.202100587

World Health Organization. (2020). Food safety. World Health Organization. Retrieved August 31, 2022, from https://www.who.int/news-room/fact-sheets/detail/food-safety

Xiao, Y., Liu, Y., Kang, S., Wang, K., & Xu, H. (2020). Development and evaluation of soy protein isolatebased antibacterial nanocomposite films containing cellulose nanocrystals and zinc oxide nanoparticles. *Food Hydrocolloids, 106*, 105898. https://doi.org/10.101 6/j.foodhyd.2020.105898

Xie, D., Weng, Y., Guo, X., Zhao, J., Gregory, R. L., & Zheng, C. (2011). Preparation and evaluation of a novel glass-ionomer cement with antibacterial functions. *Dental Materials, 27*(5), 487-496. https://doi.org/10.1016/j.dental.2011.02.006

Xu, D., Wang, S., Hu, J., Liu, Y., Jiang, Z., & Zhu, P. (2021). Enhancing antibacterial and flame-retardant performance of cotton fabric with an iminodiacetic acid-containing N-halamine. *Cellulose, 28*(5), 3265-3277. https://doi.org/10.1007/s10 570-021-03716-x

Xu, Z., Pan, N., Xue, Y., Jiang, T., & Wang, Y. (2022). Long-lasting renewable antibacterial graphene/N-halamine-coated cotton fabrics benefitting from enhanced UV stability and quantitative tracking of bactericidal factors. *International Journal of Biological Macromolecules, 222*, 1192-1200. https://doi.org/10.1016/j.ijbiomac.2022.09.254

Yu, F., Fei, X., He, Y., & Li, H. (2021). Poly(lactic acid)-based composite film reinforced with acetylated cellulose nanocrystals and ZnO nanoparticles for active food packaging. *International Journal of Biological Macromolecules, 186*, 770-779. https://doi.org/10.1016/j.ijbiomac.2021.07.097

Zhang, H., Hortal, M., Jordá-Beneyto, M., Rosa, E., Lara-Lledo, M., & Lorente, I. (2017). ZnO-PLA nanocomposite coated paper for antimicrobial packaging application. *LWT, 78*, 250-257. https://doi.org/10.1016/j.lwt.2016.12.024

Zhang, R., Lan, W., Ji, T., Sameen, D. E., Ahmed, S., Qin, W., & Liu, Y. (2021). Development of polylactic acid/ZnO composite membranes prepared by ultrasonication and electrospinning for food packaging. *LWT, 135*, 110072. https://doi.org/10.1016/j.lwt.20 20.110072

Zhang, X., Zhang, Q., Xue, Y., Wang, Y., Zhou, X., Li, Z., & Li, Q. (2021). Simple and green synthesis of calcium alginate/AgCl nanocomposites with low-smoke flame-retardant and antimicrobial properties. *Cellulose*, *28*(8), 5151-5167. https:// doi.org/10.1007/s10570-021-03825-7

Zhao, S.-W., Zheng, M., Zou, X.-H., Guo, Y., & Pan, Q.-J. (2017). Self-Assembly of Hierarchically Structured Cellulose@ZnO Composite in Solid–Liquid Homogeneous Phase: Synthesis, DFT Calculations, and Enhanced Antibacterial Activities. *ACS Sustainable Chemistry & Engineering, 5*(8), 6585-6596. https://doi.org/10.1021/acs suschemeng.7b00842

Zhong, C., Hou, P.-F., Li, Y.-X., Yang, W.-Y., Shu, M., & Wu, G.-P. (2021). Characterization, antioxidant and antibacterial activities of gelatin film incorporated with protocatechuic acid and its application on beef preservation. *LWT, 151*, 112154. https://doi.org/10.10 16/j.lwt.2021.112154

Zhou, C., Girouard, F., O'Brien, B., Ronholm, J., & Wang, Y. (2022). Construction of chevaux-de-frise from cellulose nanocrystals to enable mechano-bactericidal activity on recycled waste cotton films. *Green Chemistry, 24*(3), 1109-1113. https://doi.org/10.10 39/d2gc00073c

Zhou, Q., Chen, J., Wang, C., Yang, G., Janaswamy, S., Xu, F., & Liu, Z. (2022). Preparation and characterization of lignin nanoparticles and chitin nanofibers reinforced PVA films with UV shielding properties. *Industrial Crops and Products, 188*, 115669. https://doi.org/10.1016/j.indcrop.2022.115669

Zhou, X., Cheng, R., Wang, B., Zeng, J., Xu, J., Li, J., Kang, L., Cheng, Z., Gao, W., & Chen, K. (2021). Biodegradable sandwich-architectured films derived from pea starch and polylactic acid with enhanced shelf-life for fruit preservation. *Carbohydrate Polymers, 251*, 117117. https://doi.org/10.1016/j.carbpol.2020.117117

722 **Graphical abstract**

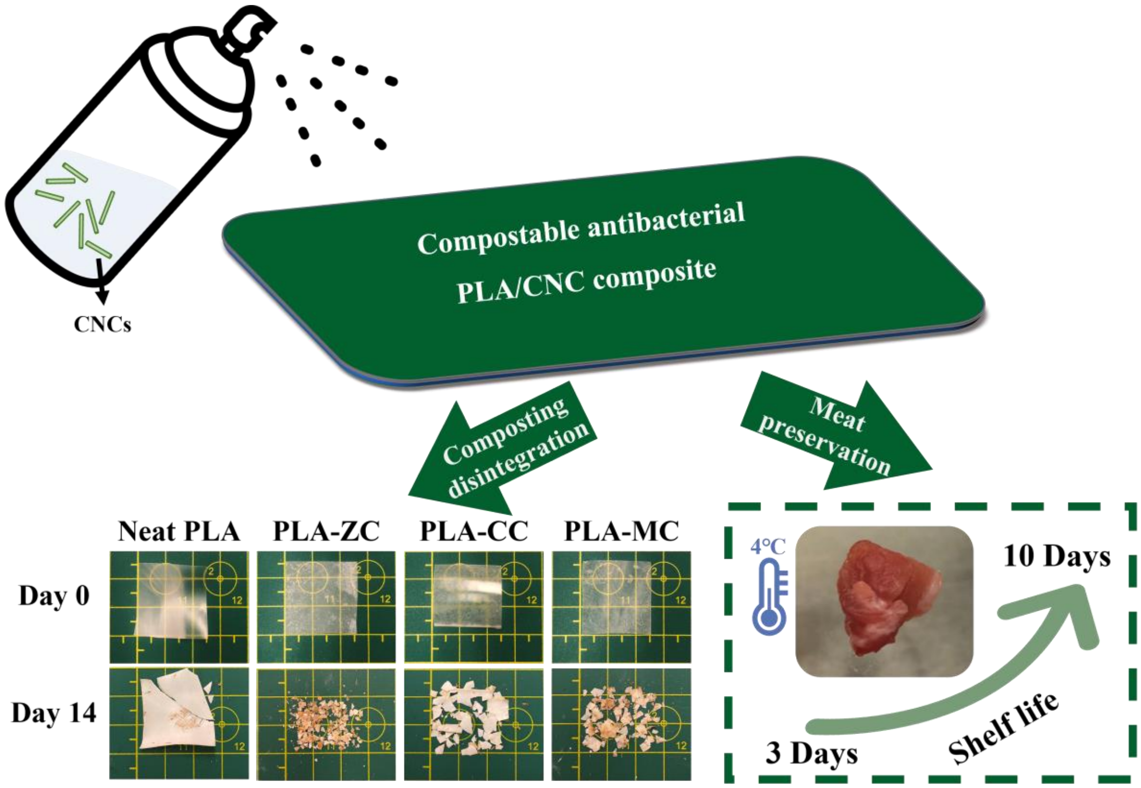

723